

Minimum Volume Enclosing Ellipsoid for Object Location

KAIBO FAN, PING WANG

School of Electrical and Information Engineering

Tianjin University

Weijin Road 92, 300072 Tianjin

CHINA

fankaibo@tju.edu.cn

Abstract: - In this work, we present a novel optimizing approach to the problem of human body location in video surveillance. The pixels of the object extracted by background subtraction technique are grouped into a point set. It can be covered by an optimal ellipsoid with the minimum enclosing volume. The task of constructing the minimum volume enclosing ellipsoid (MVEE) is implemented by convex optimization theory. We get the parameters of the minimum volume enclosing ellipsoid by solving the problem of the dual formation of the MVEE. Compared with the traditional geometrical moment based method and enclosing box, our approach gives a better result in terms of computing time and object locating affinity. The computing time of the proposed method is only 5.1% and 9.7% of the time used up by the geometrical moment based method and the enclosing box, respectively. The object locating affinity is 10.0% and 8.2% higher than that of the two compared methods.

Key-Words: - video surveillance, fall detection, object location, minimum volume enclosing ellipsoids

1 Introduction

The minimum volume enclosing ellipsoids (MVEE) problem has been studied since it was first discussed in connection with optimality conditions. The problem consists of covering a set of points $\{x_1, x_2, \dots, x_m\} \in R^n$ with an ellipsoid of minimum volume. It can be found in various formulations, each of them presenting different properties [1]. The most simple formulation is the center form described by a symmetric matrix $E \in R^{n \times n}$ and a center of the ellipsoid, i.e.,

$$\varepsilon_{E,c} = \{x \in R^n \mid (x-c)^T E (x-c) \leq 1\}$$

Its shape is determined by the symmetric matrix E . The volume of $\varepsilon_{E,c}$ is given by the formula

$$\pi^{n/2} \Gamma^{-1}(n/2 + 1) \det(E^{-1/2})$$

where $\Gamma(n)$ is the gamma function. Minimum volume enclosing ellipsoids also play an important role in several diverse spheres of application such as optimal design [2], human computer interaction [3, 4], convex optimization [5], anomaly detection [6, 7], pattern recognition [8, 9] and statistics [10, 11].

In this paper, we are going to locate the extracted area of a moving human body in the image plane by a minimum volume ellipsoid. It is a key step in analysing the behaviour of a monitored person, especially in the video surveillance and home assistant robot. In order to extract the objects in

foreground image, a background model is established firstly. The moving objects can be extracted by the background subtraction technique. After detecting the object in the foreground image, one way of finding the extracted object is counting the number of pixels belonging to the object. It is often used to locate the objects in the digital image processing community. The result is promising when there is a holistic object in the image plane. Sometimes, this method only finds the largest component of the object, because it can not cope with the fragmented object in the image. Additionally, it is very sensitive to the noises.

The alternative method is to employ an ellipsoid covering the object. To the best of our knowledge, it is the first time when the optimization techniques are used to locate a moving object in an image sequence. The problem of locating the foreground object, represented as a point set, can be solved by constructing a minimum area enclosing ellipsoid. The region of the object can be located very well in the image plane. By this method, we can also get an approximate shape of the human body by covering the points in the minimum enclosing volume ellipsoid.

The remainder of the paper is organized as follows. In Section 2, we briefly describe the foreground segmentation implemented with the help of a background model. Section 3 gives an elaborate explanation of the process of locating an object by approximated ellipsoid, and includes the description

of optimizing the model of the MVVEE, calculating the parameters of the covering ellipsoid and moment based ellipsoid. In Section 4, we present the computational results, evaluate the performance of the proposed algorithm in the aspects of computing time and object locating affinity. Finally, Section 5 contains the conclusion.

2 Foreground segmentation

Extracting the moving objects from image sequences is the prerequisite of our object locating method. Human is one of the most critical object to be considered in video surveillance. However, the moving human body is an extremely non-rigid object with a high degree of variability in size and shape. When people walk towards a video camera or away from it, both the shape and size of a human body change a lot. Sometimes, even the color and texture are effected greatly by the shadow or ambient light in a living room. A visual extractor has to deal with such complex situations.

To accomplish this goal, we use a background subtraction method described in [12], which gives appropriate results on image sequences with shadows, highlights, and high image compression.

2.1 Color distortion model

For the color distortion model, N ($N = 30$ in this paper) static background images are used to construct a background image. There is a difference between the current point $I(i) = \{I_R(i), I_G(i), I_B(i)\}$ and the background point $E(i) = \{E_R(i), E_G(i), E_B(i)\}$. After subtracting the current image from the background, we use statistics derived by a distance function to measure the difference between the values of pixels in a current image and the background image. The statistics are also used to determine the thresholds. According to these thresholds, the current pixels are classified into different object masks. To solve this problem, we take a scalar instead of three-color components for the brightness.

The line starting from the origin and passing through the point $E(i)$ represents the brightness of the point in the background. This brightness is scaled by a factor $\alpha(i)$. If $\alpha(i)$ exceeds one, the point is brighter, if it is less than one, the point is darker. So, $\alpha(i)$ is a measure of the brightness difference between the current point $I(i)$ and the reference point $E(i)$. The brightness distortion

$BD(\alpha(i))$ is the value of $\alpha(i)$ which brings the observed color close to the line $\overline{OE(i)}$, as follows

$$BD(\alpha(i)) = \min \|I(i) - \alpha(i)E(i)\|_2^2 \quad (1)$$

Then we obtain the chrominance distortion $CD(i)$ as the distance of $I(i)$ from $\alpha(i)E(i)$

$$CD(i) = \|I(i) - \alpha(i)E(i)\|_2 \quad (2)$$

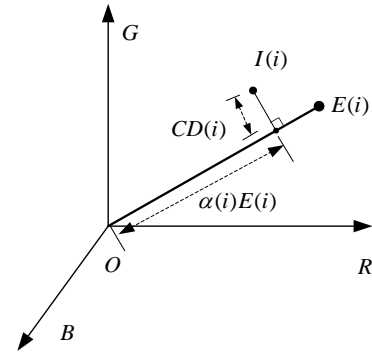


Fig. 1. Colour distortion model

This is illustrated in Fig. 1, where the chrominance distortion is the length of the line normal to line $\overline{OE(i)}$. The algorithm initially uses N frames to construct the background model and to obtain the mean and the standard deviation for each pixel. The expected color $E(i)$ is the average over these N frames $E(i) = \{\mu_R(i), \mu_G(i), \mu_B(i)\}$ and the standard deviation $s(i)$ is the variance $s(i) = \{\sigma_R(i), \sigma_G(i), \sigma_B(i)\}$ of them.

The value of $\alpha(i)$ is that which minimizes

$$\min \left\{ \sum_{C \in \{R, G, B\}} \left(\frac{I_C(i) - \alpha(i)\mu_C(i)}{\sigma_C(i)} \right)^2 \right\} \text{ giving}$$

$$BD(\alpha(i)) = \frac{\sum_{C \in \{R, G, B\}} \left(\frac{I_C(i)\mu_C(i)}{\sigma_C^2(i)} \right)}{\sum_{C \in \{R, G, B\}} \left(\frac{\mu_C(i)}{\sigma_C(i)} \right)^2} \quad (3)$$

and

$$CD(i) = \sqrt{\sum_{C \in \{R, G, B\}} \left(\frac{I_C(i) - \alpha(i)\mu_C(i)}{\sigma_C(i)} \right)^2} \quad (4)$$

Different pixels yield different distributions of $\alpha(i)$ and $CD(i)$. Having known these

characteristics of the distributions, we can deduce appropriate classification thresholds.

The variations of the brightness distortion and chrominance distortion are given by

$$a(i) = \text{RMS}(\alpha(i)) = \sqrt{\frac{\sum_{i=1}^N (\alpha(i)-1)^2}{N}} \quad (5)$$

$$b(i) = \text{RMS}(CD(i)) = \sqrt{\frac{\sum_{i=1}^N (CD(i))^2}{N}}$$

Then normalize the values of $BD(\alpha(i))$ and $CD(i)$ in the same range just as $a(i)$ and $b(i)$

$$\hat{BD}(\alpha(i)) = \frac{BD(\alpha(i))-1}{a(i)} \quad (6)$$

$$\hat{CD}(i) = \frac{CD(i)}{b(i)}$$

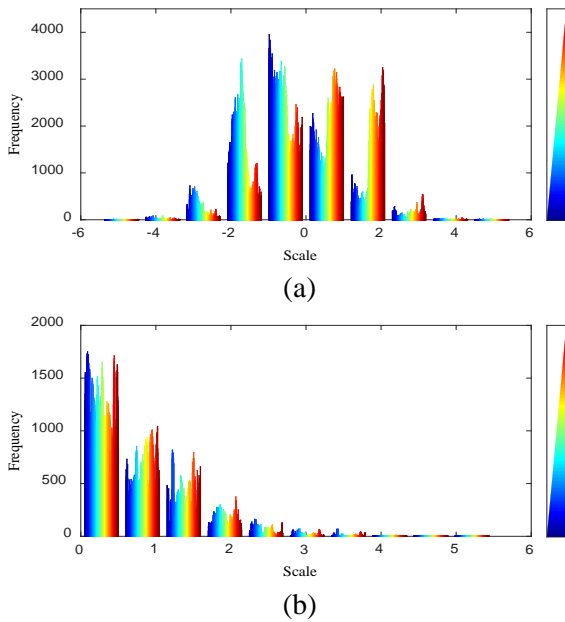


Fig. 2. Brightness and chromaticity distortion of background. (a) Normalized brightness distortion. (b) Normalized chromaticity distortion.

Fig. 2 demonstrates the distributions of $\hat{BD}(\alpha(i))$ and $\hat{CD}(i)$ of the background. It reflects the brightness and chromaticity fluctuation of background. The distributions of $\hat{BD}(\alpha(i))$ and $\hat{CD}(i)$ of the background can be used to determine the thresholds for pixel classification.

2.2 Pixel classification

By analyzing the characteristics of chrominance and brightness, the pixels in the current image can be classified into one of the three categories:

- The background B : if the brightness and chrominance are similar to those of the original image.
- The shadow S : if it has similar chrominance but the lower brightness.
- The moving (foreground) object F : if it has different chrominance.

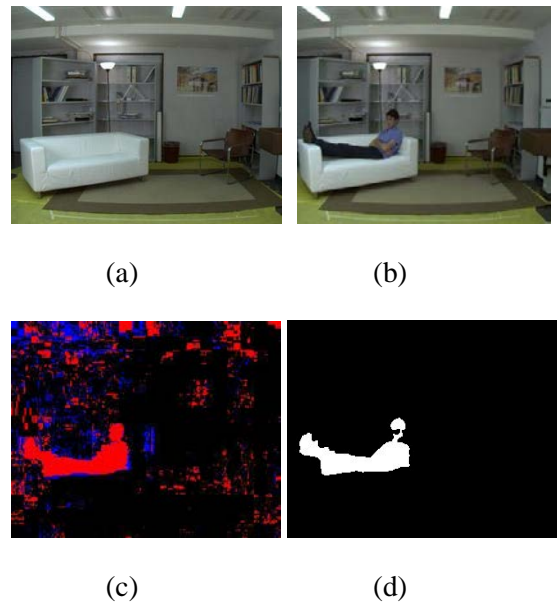


Fig. 3. Human body extraction. (a) An original background image. (b) The current image with a human body. (c) The extracted human body in a foreground including shadows and holes. (d) The final extracted human object after the morphological operations.

This is achieved by using thresholds for $\hat{BD}(\alpha(i))$ and $\hat{CD}(i)$. Then the pixels in the current image are classified into a set of labels as

$$M(i) = \begin{cases} F : \text{if } \hat{CD}(i) < T_{CD} \\ B : \text{if } T_{BD_{low}} < \hat{BD}(\alpha(i)) < T_{BD_{high}} \\ S : \text{if } \hat{BD}(\alpha(i)) < 0 \end{cases} \quad (7)$$

The background subtraction is illustrated in Fig. 3.

After the foreground segmentation is done, in order to gain a deeper understanding of the human motions we should proceed to locate the region of the moving object on the image plane. Then, the

analysis of the human body shape in that located region is performed to detect the changes in its orientation and proportion. For that purpose, the best choice is to use an ellipsoid for the shape approximation. We consider that this representation of the human object good enough for distinguishing different movements of the monitored person. It is also adequate for tracking out a wide range of postures and clothing.

3 Ellipsoid approximation

In this section, we present two different methods for computing the covering ellipsoid of a point set. The first method makes use of minimum volume ellipsoids. The ellipsoid is formulated in the center form, i.e., the center $c \in R^n$ and the symmetric matrix $E \in R^{n \times n}$. The center and symmetric matrix of the ellipsoid are obtained by minimizing the volume of the ellipsoid. The second approach uses the first and second moments of the data points to calculate the parameters of an ellipsoid that covers most of the points.

3.1 Minimum volume enclosing ellipsoid

Practically, a foreground object is usually separated into several small blocks, since it moves rapidly on the similar background along with the human body. We gather all the extracted pixels together into a point set, and identifying of the human body in the image plane can be carried out by optimizing the minimum area enclosing ellipsoid of these points.

Suppose a set of m point in n dimensional space $S = \{x_1, x_2, \dots, x_m\} \in R^n$. Let us denote the minimum volume enclosing ellipsoid of the set S $MVEE(S)$. In order to guarantee that any ellipsoid containing S has positive volume, we assume that the affine hull of x_1, x_2, \dots, x_m spans R^n .

Definition 1 An ellipsoid in the center form is given by

$$\mathcal{E}_{E,c} = \{x \in R^n \mid (x-c)^T E(x-c) \leq 1\}$$

where $c \in R^n$ is the center of the ellipsoid $\mathcal{E}_{E,c}$ and $E \in S_{++}$. S_{++} is the convex cone of $n \times n$ symmetric positive matrixes.

Since we hope all the points x_i to be inside $\mathcal{E}_{E,c}$, they should satisfy the following constraint

$$(x_i - c)^T E(x_i - c) \leq 1 \quad i = 1, 2, \dots, m \quad (8)$$

The volume of $\mathcal{E}_{E,c}$ is given by

$$\text{Vol}(\mathcal{E}_{E,c}) = \frac{\eta}{\sqrt{\det(E)}} = \eta \det(E^{-\frac{1}{2}}) \quad (9)$$

where η is the volume of the unit ball in R^n and can be computed by a gamma function $\Gamma(n)$ [13]. Thus, the problem of determining the ellipsoid of the least volume containing the points of S is equivalent to finding a vector $c \in R^n$ and a $n \times n$ positive definite symmetric matrix E that minimizes $\det(E^{-1})$ under the constraint equation (8).

A mathematical formulation of the problem is given as follows

$$\begin{aligned} \min_{E,c} \quad & \det(E^{-1}) \\ \text{s.t.} \quad & (x_i - c)^T E(x_i - c) \leq 1 \\ & i = 1, 2, \dots, m \\ & E \succ 0 \end{aligned} \quad (10)$$

where \succ means a positive definite matrix restriction. It is not a convex optimization problem. By making an appropriate change of variable, we can reformulate the problem as

$$\mathcal{E}_{E,c} = \{x \in R^n \mid \|Ax - b\|_2 \leq 1\}$$

where $A = E^{\frac{1}{2}}$ and $b = E^{\frac{1}{2}}c$. Thus, the minimum volume enclosing ellipsoid problem (10) becomes

$$\begin{aligned} \min_{A,b} \quad & -\log \det(A) \\ \text{s.t.} \quad & \|Ax_i - b\|_2 \leq 1 \\ & i = 1, 2, \dots, m \\ & A \succ 0 \end{aligned} \quad (11)$$

The norm constraints $\|Ax_i - b\|_2 \leq 1$ are just convex quadratic inequalities in the variables A and b . It can be expressed as linear matrix inequalities

$$\begin{bmatrix} I & Ax_i - b \\ (Ax_i - b)^T & \mathbf{1} \end{bmatrix} \succeq 0$$

Therefore, problem (11) is a convex problem in variables A and b . However, it is difficult to solve this problem directly. It proves that the dual problem is easier than the primal problem. We modify the primal problem (10) and proceed to solve it in this way.

3.1.1 Dual formulation and solution

Definition 2 A set of m point in n dimensional space $S = \{x_1, x_2, \dots, x_m\} \in R^n$. The lifting set of S is formulated as $S' = \{\pm q_1, \dots, \pm q_m\} \in R^{n+1}$, where $q_i^T = [x_i^T, 1]$, $i = 1, \dots, m$.

By this definition each point x_i is lifted to the hyperplane $H = \{(x, x_{n+1}) \in R^{n+1} | x_{n+1} = 1\}$. Since S' is centrally symmetric, $MVEE(S')$ is centered at the origin of the hyperplane. From the result of [15], the minimum volume enclosing ellipsoid of the original problem is recovered as the intersection of H with the minimum volume enclosing ellipsoid that contains the lifted points q_i of the set S'

$$MVEE(S) = MVEE(S') \cap H$$

The lifted primal problem is as follows

$$\begin{aligned} \min_M \quad & -\log \det(M) \\ \text{s.t.} \quad & q_i^T M q_i \leq 1 \\ & i = 1, 2, \dots, m \\ & M \succ 0 \end{aligned} \tag{12}$$

where $M \in S_{++}^{(n+1)}$ is the decision variable.

Let P denote the $n \times m$ matrix whose columns are the vectors p_i , i.e., $P = [p_1, \dots, p_m]$, then the matrix Q whose columns are the vectors q_i is given by

$$Q = [q_1, \dots, q_m] = \begin{bmatrix} P \\ \mathbf{1}^T \end{bmatrix} \in R^{(n+1) \times m}$$

The Lagrangian dual problem is given by

$$\begin{aligned} \max_\lambda \quad & \log \det V(\lambda) \\ \text{s.t.} \quad & \mathbf{1}^T \lambda = n + 1 \\ & \lambda \succeq 0 \end{aligned} \tag{13}$$

where $V(\lambda) = Q \text{diag}(\lambda) Q^T$ and $\lambda \in R^m$ is the decision variable. The change of variable $\lambda = (n + 1)u$ results in the following dual problem

$$\begin{aligned} \max_u \quad & \log \det V(u) \\ \text{s.t.} \quad & \mathbf{1}^T u = 1 \\ & u \succeq 0 \end{aligned} \tag{14}$$

where $V(u) = QUQ^T$ and $U = \text{diag}(u) \in R^{m \times m}$.

Problem (14) is a concave optimization problem, so we can apply an ascent method [16] to find the optimal u^* .

3.1.2 Computing the parameters of the covering ellipsoid

Considering the primal problem (12) with the lifted points q_i of the set S' , the Lagrangian function is given by

$$L(M, \lambda) = -\log \det M + \sum_{i=1}^m \lambda_i (q_i^T M q_i - 1)$$

Under the Karush-Kuhn-Tucker (KKT) conditions for optimality, we have

$$\frac{\partial L}{\partial M} = -M^{-1} + \sum_{i=1}^m \lambda_i q_i q_i^T = -M^{-1} + Q \Lambda Q^T$$

where $\Lambda = \text{diag}(\lambda)$ and $Q = [q_1, \dots, q_m]$. It implies that when a positive definite matrix $M^* \in R^{(n+1) \times (n+1)}$ is optimal for the primal problem (12) with the Lagrangian multipliers $\lambda^* \in R^m$, then we have

$$V(\lambda^*) = Q \Lambda^* Q^T = (M^*)^{-1} = (n + 1)V(u^*)$$

Since $q^T = [x^T, 1]$, the equation of the ellipsoid is given by

$$\begin{aligned} MVEE(S) &= \{x \in R | q^T M^* q \leq 1\} \\ &= \{x \in R | (\frac{1}{n+1}) q^T V(u^*)^{-1} q \leq 1\} \end{aligned}$$

Therefore, we can find the equation of the ellipsoid under the solution of dual the problem (13). Note that we have

$$V(u) = QUQ^T = \begin{bmatrix} PUP^T & Pu \\ (Pu)^T & \mathbf{1}^T u \end{bmatrix}$$

which can be factorized as

$$V(u) = \begin{bmatrix} I & Pu \\ 0 & 1 \end{bmatrix} \begin{bmatrix} E^{-1} & 0 \\ 0 & 1 \end{bmatrix} \begin{bmatrix} I & 0 \\ (Pu)^T & 1 \end{bmatrix}$$

where $E^{-1} = PUP^T - Pu(Pu)^T$. The inverse $V(u)^{-1}$ is given by

$$V(u)^{-1} = \begin{bmatrix} I & 0 \\ -(Pu)^T & 1 \end{bmatrix} \begin{bmatrix} E & 0 \\ 0 & 1 \end{bmatrix} \begin{bmatrix} I & -Pu \\ 0 & 1 \end{bmatrix}$$

Thus, we get $q^T V(u)^{-1} q = (x - Pu)^T E (x - Pu)$.

As for the dual optimal solution u^* , we have

$$MVEE(S) = \{x \in R^n | (x - c^*)^T E^* (x - c^*) \leq 1\}$$

$$\begin{aligned} E^* &= \frac{1}{n} (PU^* P^T - Pu^* (Pu^*)^T)^{-1} \\ c^* &= Pu^* \end{aligned} \tag{15}$$

3.2 Moment based ellipsoid

Definition 3 For a continuous image $f(x, y)$, the moments are given by

$$m_{pq} = \int_{-\infty}^{+\infty} \int_{-\infty}^{+\infty} x^p y^q f(x, y) dx dy$$

for $p, q = 0, 1, \dots$

The center of the ellipsoid (\bar{x}, \bar{y}) is obtained by computing the coordinates of the center of mass with the first and zero order spatial moments

$$\begin{aligned} \bar{x} &= m_{10} / m_{00} \\ \bar{y} &= m_{01} / m_{00} \end{aligned} \quad (16)$$

Definition 4 For a continuous image $f(x, y)$, and its centroid (\bar{x}, \bar{y}) , the central moments are computed as follows

$$\mu_{pq} = \int_{-\infty}^{+\infty} \int_{-\infty}^{+\infty} (x - \bar{x})^p (y - \bar{y})^q d(x - \bar{x}) d(y - \bar{y})$$

for $p, q = 0, 1, \dots$

The angle θ between the major axis a and the horizontal axis x gives the orientation of the ellipsoid. It can be computed with the central moments of the second order

$$\theta = \frac{1}{2} \arctan\left(\frac{2\mu_{11}}{\mu_{20} - \mu_{02}}\right) \quad (17)$$

To recover the major semi-axis a and the minor semi-axis b of the ellipsoid, we have to compute I_{min} and I_{max} , the least and greatest moments of inertia, respectively. They can be computed by evaluating the eigenvalues of the covariance matrix [14]

$$J = \begin{pmatrix} \mu_{20} & \mu_{11} \\ \mu_{11} & \mu_{02} \end{pmatrix} \quad (18)$$

The eigenvalues I_{min} and I_{max} are given by

$$\begin{aligned} I_{min} &= \frac{\mu_{20} + \mu_{02} - \sqrt{(\mu_{20} - \mu_{02})^2 + 4\mu_{11}^2}}{2} \\ I_{max} &= \frac{\mu_{20} + \mu_{02} + \sqrt{(\mu_{20} - \mu_{02})^2 + 4\mu_{11}^2}}{2} \end{aligned} \quad (19)$$

Then the major semi-axis a and the minor semi-axis b of the best fitting ellipsoid are given by

$$\begin{aligned} a &= \left(\frac{4}{\pi}\right)^{1/4} \left[\frac{(I_{max})^3}{I_{min}}\right]^{1/8} \\ b &= \left(\frac{4}{\pi}\right)^{1/4} \left[\frac{(I_{min})^3}{I_{max}}\right]^{1/8} \end{aligned} \quad (20)$$

4 Computational experiments

In this section, we show the performance of the proposed algorithm. The experiments have been carried out on a desktop with Intel (R) Core (TM) i3-2120 CUP and 2.00 GB RAM. We tested it intensively on a public fall detection dataset [17]. The video sequence was recorded with static cameras at a frame rate of fifteen frames per second. It is mainly used to test our algorithm in the first step of locating a falling person during a fall incident. A fall is inherently a motion that lasts for a short period. During this period, there is a variety of postures. For the fall event analysis to be carried out effectively every posture should be located accurately on the foreground image.

Concerning the point set for the body shape approximation, the background subtraction algorithm is applied to extract the human body from each frame. The region of interest, i.e., the moving human body, is covered by the approximated ellipsoid. In order to demonstrate our algorithm, we give a sequence of a falling human with different typical postures during the fall incident. This procedure contains four different phases of a fall event, which are the pre-fall phase, critical phase, post-fall phase and recovery phase [18]. The first phase corresponding to daily life motions (like walking and so on) is illustrated by the first frame in Fig. 4(a), where it is represented by a stand posture at the beginning of the fall incident. The second critical phase corresponding to the actual fall is extremely short. It is shown in the second frame of Fig. 4(a), where it is represented by more complicated bent posture with a hole in the middle of the human body. This phase can be detected by the movement of the body toward the ground or by the ground impact. The post-fall phase during which a person is generally lying motionless on the ground is illustrated by the frames three and four of Fig. 4(a), where it is represented by a lying posture. It can be detected by a lying position or by an absence of motion. The last phase, i.e., recovery phase of the fall incident, when the person is eventually able to stand up alone or with the help of another person, is shown in the last two frames of the Fig. 4 (a). It is represented here by a limp posture when a fallen

person tries to stand up after a fall event. Note that in Fig.4(c) (the green ellipsoid), our method locates the human postures very well in all cases. In order to evaluate our algorithm, we choose some images from the fall event to compare with the geometrical moments method [19] and enclosing box [20] in

terms of computing time and object locating affinity (the ratio between the object area in the ellipsoid and the whole area of the ellipsoid).

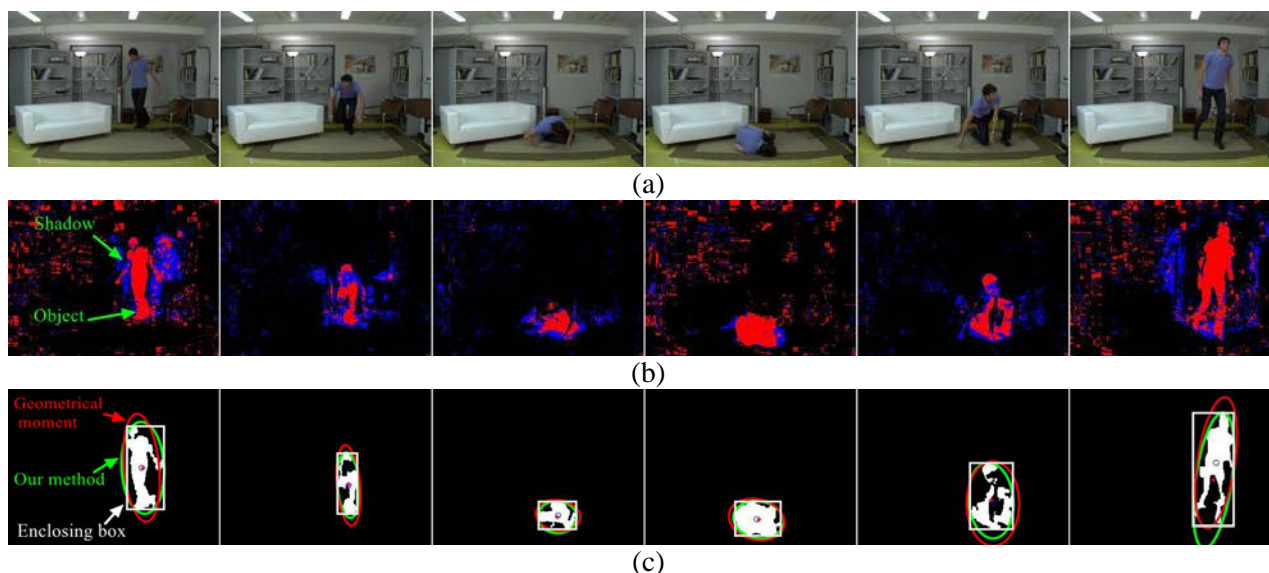


Fig. 4. A sequence of a fall incident. (a) Original typical frames of the chosen fall sequence. (b) Extracted typical postures of the chosen fall sequence. (c) The results given by different object locating algorithms.

From the comparative results in Table 1, it can be seen that the computing time of our algorithm is merely 1.00 milliseconds, which is only 5.1% and 9.7% of the time given by the geometrical moment based method and the enclosing box, respectively. The object locating affinity in Table 2 is 10.0% and 8.2% higher than that of the two compared approaches.

The application of the compared geometrical moments method in Fig. 4(c) (the red ellipsoid) requires the computing of the first and second order spatial moments and central spatial moments of the foreground image. The spatial moments are used to calculate the parameters of the locating ellipsoid, i.e., the region of interest. This is a time-consuming step. The enclosing box in Fig. 4(c) (the white rectangle) searches the foreground image and finds the minimum enclosing rectangle. It has to traverse all the points in the foreground image to find the coordinates of the rectangle. The time of locating the object in the rectangle is less than that of the geometrical moments. But the region covered by the minimum enclosing box is larger than that of the minimum ellipsoid. In the pre-fall phase, most of the postures are standing. The enclosing box can fit the body shape just like the minimum ellipsoid. Meanwhile, the bending posture always occurs in

the second phase of the fall incident. When the person tilts backward or forward, the enclosing box is not suitable for fitting the shape of the human body.

The principle of our approach is quite different from the compared two methods. After detecting the points in the foreground image, we just solve the symmetric matrix E and the center c as described in the previous section. The area of the minimum ellipsoid is affected not only by the number and the location of foreground points detected in the image plane but also by the calculation error. In practice, not all of the points are covered by the ellipsoid. Because of the round-off error, there are few points out of the minimum ellipsoid in the boundary. But this will not result in too many errors. The geometrical moment based ellipsoid encloses most of the points, but far from all. According to this method, the area is determined by the least and the greatest moments of inertia which are greatly affected by distribution of the scattered points. Its area is slightly larger than that of the corresponding minimum ellipsoid. The affinity is about 8.2% less than that of our method. Thus, our method is more effective and accurate than the traditional methods

in locating the moving human body during the fall detection.

Table 1. Locating affinity comparison results of the three methods

Images	Geometrical moment (%)	Enclosing box (%)	Our method (%)
Images1	44.94	43.80	46.75
Images2	41.07	50.36	57.44
Images3	54.6	48.75	61.29
Images4	63.99	74.55	84.05
Images5	29.89	36.94	41.82
Images6	46.95	37.84	49.79
Average	46.91	48.71	56.86

Table 2. Time comparison results of the three methods

Images	Geometrical moment (ms)	Enclosing box (ms)	Our method (ms)
Images1	19.68	10.09	1.16
Images2	19.59	10.15	0.93
Images3	19.83	10.77	0.66
Images4	19.71	9.69	0.49
Images5	19.56	10.11	1.24
Images6	19.92	10.47	1.51
Average	19.72	10.35	1.00

5 Conclusion

In this paper, we proposed a novel optimizing approach to the problem of locating the moving human object in the foreground image. The moving human body was firstly extracted by the background subtraction technique. All the pixels of the object were aggregated into a point set which was covered by a minimum volume ellipsoid. The minimum volume ellipsoid was formulated as a convex optimization problem with inequality constraint. It is not easy to solve this primal problem directly. We modified this primal problem and then solved its

dual formation to obtain the parameters of the minimum volume ellipsoid. The computational results show that the minimum volume ellipsoid represents a satisfactory solution to the problem of locating the moving human body. The computational efficiency of our method is more than ten times higher than that of the compared enclosing box and geometrical moment based ellipsoid methods.

Acknowledgements: The research was supported by the Tianjin University in the case of

the first author; it was also supported by the Department of Science and Technology in Hebei Province (grant No. 12213519D1). The authors would like to thank Dr. Fabian Nater for providing the video sequence.

References:

- [1] S. Boyd, and L. Vandenberghe, *Convex optimization*, Cambridge University Press, Cambridge, 2004.
- [2] S. Silvey, *Optimal design: an introduction to the theory for parameter estimation*, Springer, New York, 2013.
- [3] J. Music, M. Cecic, and M. Bonkovic, Testing inertial sensor performance as hands-free human-computer interface, *WSEAS T. Computers*. 8(4), 2009, pp. 715–724.
- [4] J. Music, M. Cecic, and V. Zanchi, Real-time body orientation estimation based on two-layer stochastic filter architecture, *Automatika*. 51(3), 2010, pp. 264–274.
- [5] P. Kumar, and E. A. Yildirim, Computing minimum-volume enclosing axis-aligned ellipsoids, *J. Optimiz. Theory App.* 136(2), 2008, pp. 211–228.
- [6] G. Groszklos, and J. Theiler, Ellipsoids for anomaly detection in remote sensing imagery, *Conference on Algorithms and Technologies for Multispectral, Hyperspectral, and Ultraspectral Imagery XXI*. 2015, pp. 351–370.
- [7] H. Lee, D. Moon, I. Kim, H. Jung, and D. Park, Anomaly intrusion detection based on hyper ellipsoid in the kernel feature space, *KSII T. Internet Inf.* 9(3), 2015, pp. 1173–1192.
- [8] S. Ha, Probabilistic space-time analysis of human mobility patterns, *WSEAS T. Computers*. 21(15), 2016, pp. 222–238.
- [9] L. Källberg, and T. Larsson, Improved pruning of large data sets for the minimum enclosing ball problem, *Graph. Models*. 76(6), 2014, pp. 609–619.
- [10] D. Martinez-Rego, E. Castillo, O. Fontenla-Romero, and A. Alonso-Betanzos, A minimum volume covering approach with a set of ellipsoids, *IEEE T. Pattern Anal.* 35(12), 2013, pp. 3997–3009.
- [11] S. D. Ahipasaoglu, Fast algorithms for the minimum volume estimator, *J. Global Optim.* 62(2), 2015, pp. 351–370.
- [12] T. Horprasert, D. Harwood, and L. S. Davis, A statistical approach for real-time robust background subtraction and shadow detection, *IEEE International Conference On Computer Vision*. 1999, pp. 1–19.
- [13] M. Grötschel, L. Lovász, and A. Schrijver, *Geometric algorithms and combinatorial optimization*, Springer, New York, 2012.
- [14] M. Yu, A. Rhuma, S. Naqvi, L. Wang, and J. Chambers, A posture recognition-based fall detection system for monitoring an elderly person in a smart home environment, *IEEE T. Inf. Technol. B.* 16(6), 2012, pp. 1274–1286.
- [15] Y. Nesterov, and A. Nemirovskii, *Interior-point polynomial algorithms in convex programming*, SIAM, 1994.
- [16] J. Grandon, and I. Derpich, A Heuristic for the multi-knapsack problem, *WSEAS T. Math.* 10(3), 2011, pp. 95–104.
- [17] F. Nater, T. Tommasi, H. Grabner, G. Van, and B. Caputo, Transferring activities: updating human behaviour analysis, *IEEE International Conference on Computer Vision Workshops*. 2011, pp. 1737–1744.
- [18] B. Mirmahboub, S. Samavi, N. Karimi, and S. Shirani, Automatic monocular system for human fall detection based on variations in silhouette area, *IEEE T. Bio. Med. Eng.* 60(2), 2013, pp. 427–436.
- [19] M. Yu, A. Rhuma, S. M. Naqvi, L. Wang, and J. Chambers, A posture recognition-based fall detection system for monitoring an elderly person in a smart home environment, *IEEE T. Inf. Technol. B.* 16(6), 2012, pp. 1274–1286.
- [20] J. L. Chua, Y. C. Chang, and W. K. Lim, A simple vision-based fall detection technique for indoor video surveillance, *Signal Image Video P.* 9(3), 2015, pp. 623–633.